

# STIM1L is a new actin-binding splice variant involved in fast repetitive $\text{Ca}^{2+}$ release

Basile Darbellay,<sup>1</sup> Serge Arnaudeau,<sup>2</sup> Charles R. Bader,<sup>1</sup> Stephane Konig,<sup>2</sup> and Laurent Bernheim<sup>2</sup>

<sup>1</sup>Department of Clinical Neurosciences, University Hospital of Geneva and <sup>2</sup>Department of Basic Neurosciences, Faculty of Medicine, University of Geneva, CH-1211 Geneva 4, Switzerland

Cytosolic  $\text{Ca}^{2+}$  signals encoded by repetitive  $\text{Ca}^{2+}$  releases rely on two processes to refill  $\text{Ca}^{2+}$  stores:  $\text{Ca}^{2+}$  reuptake from the cytosol and activation of a  $\text{Ca}^{2+}$  influx via store-operated  $\text{Ca}^{2+}$  entry (SOCE). However, SOCE activation is a slow process. It is delayed by >30 s after store depletion because stromal interaction molecule 1 (STIM1), the  $\text{Ca}^{2+}$  sensor of the intracellular stores, must form clusters and migrate to the membrane before being able to open Orai1, the plasma membrane  $\text{Ca}^{2+}$  channel. In this paper, we identify a new protein,

STIM1L, that colocalizes with Orai1  $\text{Ca}^{2+}$  channels and interacts with actin to form permanent clusters. This property allowed the immediate activation of SOCE, a characteristic required for generating repetitive  $\text{Ca}^{2+}$  signals with frequencies within seconds such as those frequently observed in excitable cells. STIM1L was expressed in several mammalian tissues, suggesting that many cell types rely on this  $\text{Ca}^{2+}$  sensor for their  $\text{Ca}^{2+}$  homeostasis and intracellular signaling.

## Introduction

$\text{Ca}^{2+}$  signals are involved in many cell processes from early cell differentiation to cell death. They are encoded in frequency, amplitude, duration, and localization of cytosolic  $\text{Ca}^{2+}$  transient increases (Berridge et al., 2003). Two  $\text{Ca}^{2+}$  sources enable these signals: influxes from extracellular fluids and releases from internal stores. These two sources are interdependent, as the  $\text{Ca}^{2+}$  content of the stores is regulated by an influx from the extracellular environment by a process termed store-operated  $\text{Ca}^{2+}$  entry (SOCE).

Cellular events connecting  $\text{Ca}^{2+}$  store depletion to SOCE activation have been clarified recently with the identification of two major SOCE components: the stromal interaction molecules (STIMs) STIM1 and STIM2 and the Orai family of channels Orai1–3. STIMs are single-pass transmembrane ER  $\text{Ca}^{2+}$  sensors that activate SOCE upon  $\text{Ca}^{2+}$  store depletion (Liou et al., 2005; Roos et al., 2005; Brandman et al., 2007; Wang et al., 2009; Zhou et al., 2009). When  $\text{Ca}^{2+}$  decreases in the stores, STIMs slowly redistribute into clusters where they colocalize with Orai channels to form elementary subunits of SOCE

(Liou et al., 2005; Luik et al., 2006; Mercer et al., 2006; Treves et al., 2010). Recent publications describe specific sequences of STIMs involved in oligomerization, cluster formation, and Orai activation (Liou et al., 2005; Baba et al., 2006; Zeng et al., 2008; Fahrner et al., 2009; Muik et al., 2009; Park et al., 2009; Yuan et al., 2009).

In mammalian skeletal muscle cells, single-twitch contractions are controlled by ER  $\text{Ca}^{2+}$  releases without noticeable contribution of  $\text{Ca}^{2+}$  influxes (Lamb, 2000; Launikonis et al., 2010). However, during repetitive twitches, SOCE is required, thus providing an excellent model for studying  $\text{Ca}^{2+}$  store regulation during repetitive  $\text{Ca}^{2+}$  releases (Stiber et al., 2008; Darbellay et al., 2010). Accordingly, STIM1-deficient human patients and mice present an abnormal muscular fatigability (Stiber et al., 2008; Feske, 2009, 2010; Picard et al., 2009; Feske et al., 2010). STIM1 has been shown to be permanently localized within the triad junction of muscle fibers (Stiber et al., 2008). This may be part of the reason for the fast SOCE activation in muscle (<1 s) when compared with that of other cell types (~30 s to >1 min; Parekh and Putney, 2005; Wu et al., 2006; Launikonis and Ríos, 2007; Liou et al., 2007; Navarro-Borelly et al., 2008; Stiber et al., 2008; Calloway et al., 2009;

S. Konig and L. Bernheim contributed equally to this paper.

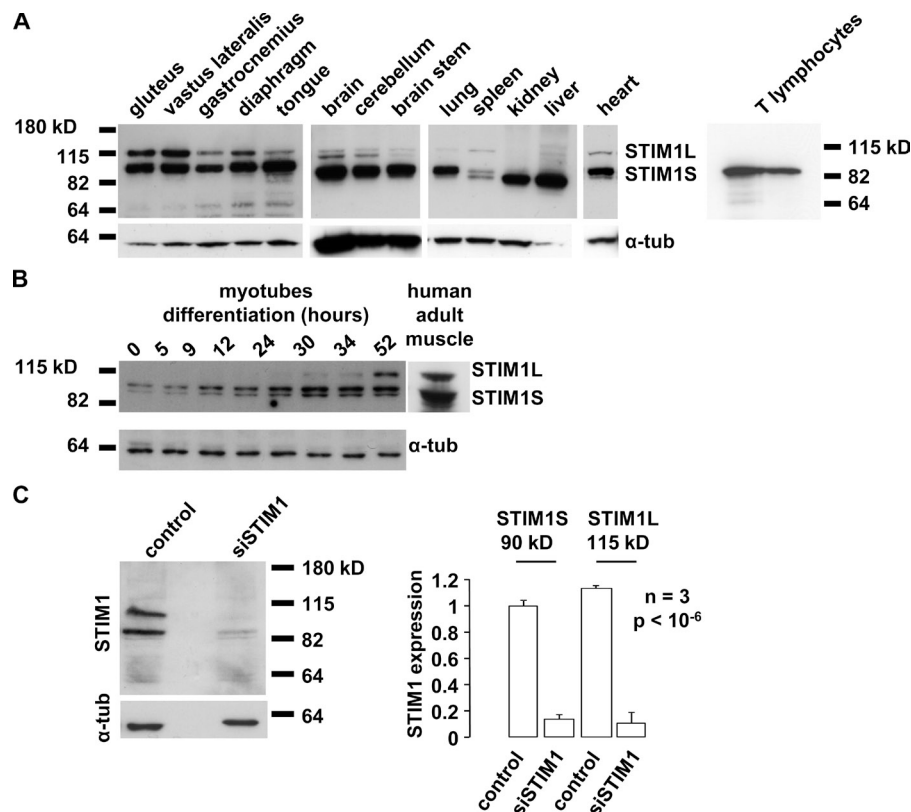
Dr. Arnaudeau died on 10 June 2010.

Correspondence to Basile Darbellay: basile.darbellay@unige.ch; or Stephane Konig: Stephane.konig@unige.ch

Abbreviations used in this paper: AM, acetoxymethyl; FRET, fluorescence resonance energy transfer; RACE, rapid amplification of 5' and 3' cDNA ends; SOCE, store-operated  $\text{Ca}^{2+}$  entry; STIM, stromal interaction molecule; Tg, thapsigargin.

© 2011 Darbellay et al. This article is distributed under the terms of an Attribution–Noncommercial–Share Alike–No Mirror Sites license for the first six months after the publication date [see <http://www.rupress.org/terms>]. After six months it is available under a Creative Commons License (Attribution–Noncommercial–Share Alike 3.0 Unported license, as described at <http://creativecommons.org/licenses/by-nc-sa/3.0/>).

**Figure 1. Identification of a new widely expressed STIM1 isoform.** (A) Expression of STIM1 splice variants (N-terminal antibody) in adult mouse tissues and in T lymphocytes of two different patients.  $\alpha$ -Tubulin ( $\alpha$ -tub) was used for a loading control. (B) STIM1 expression during myoblast differentiation and in adult human skeletal muscle (N-terminal antibody). (C, left) STIM1 expression (N-terminal antibody) 96 h after transfection with a control siRNA (control) or with an siRNA that silenced both STIM1 isoforms (siSTIM1). (right) Quantification of STIM1 silencing efficiency (mean  $\pm$  SD). STIM1 expression was normalized to control STIM1S levels and corrected for loading differences using  $\alpha$ -tubulin (also see Fig. S1 A).



Dirksen, 2009; Launikonis et al., 2009; Edwards et al., 2010). However, the molecular mechanisms underlying this fast SOCE activation are not completely understood.

In this study, we cloned a new splice variant of STIM1, STIM1L (L for long; the already well-described 90-kD STIM1 molecule will be called STIM1S in this paper), and characterized its role in cytosolic  $\text{Ca}^{2+}$  homeostasis. STIM1L triggers immediate SOCE activation upon  $\text{Ca}^{2+}$  store release and forms permanent clusters that colocalize with Orail. These permanent clusters are independent of the  $\text{Ca}^{2+}$  content of stores and rely on an interaction between STIM1L and actin fibers. As both STIM1 variants (STIM1S and STIM1L) are strongly expressed in mammalian skeletal muscle cells, we decided to mainly use human myotubes produced by in vitro differentiation to analyze the endogenous function of STIM1L. We show that in myotubes silenced for endogenous STIM1L, SOCE activation was delayed, and repetitive depolarization-induced  $\text{Ca}^{2+}$  releases were precluded as they rapidly emptied  $\text{Ca}^{2+}$  stores. On the other hand, overexpression of STIM1L in cells that do not endogenously express this protein drastically accelerated SOCE activation. We conclude that  $\text{Ca}^{2+}$  signals encoded by fast repetitive releases require the immediate activation of SOCE triggered by STIM1L.

## Results

### Two distinct STIM1 proteins are expressed in various mammalian tissues

Two STIM1 proteins of different size are expressed in most murine tissues: the well-known 90-kD STIM1 (from now on, we will refer to this protein as STIM1S, with S denoting small) and

a new 115-kD STIM1 named STIM1L (Fig. 1 A). STIM1L was detected in all tested skeletal muscles (gluteus, vastus lateralis, gastrocnemius, diaphragm, and tongue) and in the three tissues belonging to the central nervous system (brain, cerebellum, and brain stem). STIM1L was also detected in the spleen, lungs, liver, and heart but not in the kidney. Note that, as previously described (Berna-Erro et al., 2009), STIM1S is ubiquitously expressed in mouse tissues. Because STIM1L is highly expressed in all skeletal muscles (and not in T lymphocytes; Fig. 1 A), we decided to use cultured multinucleated myotubes to decipher its molecular and functional characteristics.

We first confirmed that STIM1L is expressed in adult human muscle fibers and in in vitro-differentiated myotubes. The time course of STIM1 expression during the first 52 h of myotube differentiation is illustrated in Fig. 1 B. STIM1L appeared during the second day of differentiation and is abundantly expressed in adult human semitendinous muscle. The two 90- and 115-kD proteins were recognized by three different anti-STIM1 antibodies and were both silenced by different siRNAs directed against STIM1 (small interfering STIM1 [siSTIM1]; Figs. 1 C [left] and S1 A). Western blot quantification showed that siSTIM1 reduced the expression of the 90-kD protein by  $88 \pm 6\%$  and that of the 115-kD protein by  $90 \pm 10\%$  ( $n = 3$ , and  $P < 10^{-6}$  for both conditions; Fig. 1 B, right). Collectively, these results identify STIM1L as a new member of the STIM1 protein family.

### STIM1L results from an alternative splicing on exon 11

We performed an RNA ligase-mediated rapid amplification of 5' and 3' cDNA ends (RACE) followed by PCR amplification

using STIM1-specific primers (see Materials and methods) to evaluate any possible alternative splicing on STIM1 mRNA. Only one band of the expected size (1.5 kb) was revealed by 5' end amplification of mRNA from differentiating myotubes (Fig. S1 B, left). On the other hand, 3' end amplification identified one band in mRNA from myoblasts but two bands in myotubes (Figs. 2 A and S1 B). Sequencing of both bands confirmed the specific amplification of STIM1 cDNA and identified a new sequence inserted between exons 11 and 12 of the known *stim1* human gene (available from GenBank/EMBL/DBJ under accession no. NG\_016277). This 318-bp segment aligned in silico with a sequence immediately after exon 11 in the *stim1* human gene. From these results, we conclude that during human myoblast differentiation, an alternative splicing occurs on exon 11 of STIM1, producing a new STIM1 protein characterized by a longer exon 11 encoding a longer cytosolic C-terminal tail (Fig. 2, B and C). Fig. 2 D shows the amino acid sequence of the additional segment displaying threonine- and serine-rich domains (the nucleotide sequence is shown in Fig. S1 C; available from GenBank under accession no. HQ317451). The sequence is highly conserved in mammals, suggesting that it is involved in essential functions (Fig. S2 A). Additionally, we confirmed these findings by performing PCR using primers targeting exons 10 and 12 of STIM1 (Fig. S2 B).

### STIM1L activates Orai1 upon store depletion and is involved in endogenous SOCE

To evaluate the role of STIM1L during thapsigargin (Tg)-induced SOCE, we overexpressed STIM1L in STIM1S-silenced myoblasts. Cells were cotransfected with a plasmid encoding for the ORF of STIM1L and an siRNA targeting 3' untranslated noncoding sequences of STIM1 mRNA (siSTIM1u). 2 d after transfection,  $\text{Ca}^{2+}$  handling was assessed using the fluorescent  $\text{Ca}^{2+}$  indicator Fura-2. As shown in Fig. 3 A, STIM1S silencing decreased the amplitude of SOCE evoked by readdition of 1.8 mM  $\text{Ca}^{2+}$  after depletion of the  $\text{Ca}^{2+}$  stores with 1  $\mu\text{M}$  Tg (red curve). Overexpression of STIM1L in STIM1S-silenced myoblasts more than compensated for the depletion of STIM1S and caused a  $312 \pm 20\%$  increase of the Tg-induced SOCE when compared with control myoblasts (Fig. 3 A, green curve vs. red curve). Western blots were performed on extracts obtained from the cells used for Fura-2 measurements to correlate as accurately as possible the protein levels with the  $\text{Ca}^{2+}$  influxes shown in Fig. 3 A (Fig. 3 B). As shown, proliferating myoblasts only express STIM1S, and STIM1S is silenced by  $74 \pm 7\%$  ( $n = 3$ ) 48 h after siSTIM1u transfection. As expected, in myoblasts transfected with the STIM1L plasmid and siSTIM1u, the 115-kD band was strongly expressed, whereas the amount of STIM1S decreased by  $70 \pm 11\%$  ( $n = 3$ ). From these results, we conclude that STIM1L is able to generate SOCE independently of the well-characterized SOCE partner STIM1S.

The additional sequences present on STIM1L are located near regions known to interact with Orai1 (Fig. 2). We thus wondered whether Orai1 channels would still be the main partner of STIM1L. To test this point, we quantified SOCE in

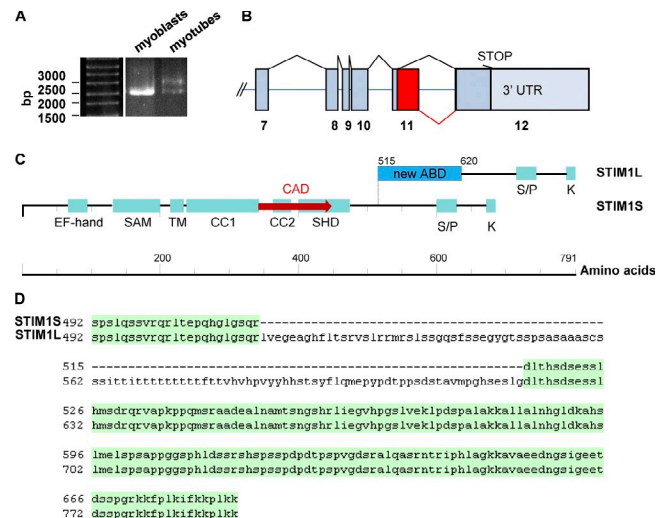


**Figure 2. STIM1 alternative splicing.** (A) Identification of an alternative splicing variant of STIM1 mRNA by RACE. Products of the 3' RACE before amplification by nested PCR are shown. 3' RACE of STIM1 mRNA was performed in proliferating myoblasts and in myotubes after 120 h of differentiation. One band of the expected size of  $\sim 2.6$  kbp was detected in myoblasts and myotubes, and an additional band of  $\sim 2.9$  kbp was detected in myotubes (also see Fig. S1 B). (B) Exon/intron map of the human 3' part of STIM1L. The spliced sequence (red) of STIM1L directly follows exon 11 of STIM1S (in silico analysis). UTR, untranslated. (C) A schematic of the proteins STIM1S and -L. ABD, actin-binding domain; CAD,  $\text{Ca}^{2+}$  release-activated  $\text{Ca}^{2+}$  channel activation domain; CC1, coiled coil 1; CC2, coiled coil 2; K, leucine-rich domain; SAM, sterile  $\alpha$  motif; SHD, STIM homomerization domain; S/P, serine-proline-rich domain; TM, transmembrane domain. (D) Amino acid sequence alignment of human STIM1S (top sequences) and STIM1L (bottom sequences). Sequences in common (exons 11 and 12) are highlighted in green (also see Figs. S1 C and S2 [A and B]).

STIM1L-overexpressing myoblasts deprived of endogenous STIM1S and treated with an siRNA directed against Orai1 (siOrai1). Fig. 3 C shows that most of the gain of function conferred by the overexpression of STIM1L in STIM1S-silenced myoblasts was reversed by Orai1 silencing (compare blue and cyan curves). This result identifies Orai1 as the main partner of STIM1L. However, as the residual SOCE in Orai1-silenced myoblasts overexpressing STIM1L (cyan curve) is approximately sevenfold larger than that observed in Orai1-silenced myoblasts not overexpressing STIM1L (green curve), our results do not exclude that STIM1L may also activate  $\text{Ca}^{2+}$  channels other than Orai1. The Western blot in Fig. 3 D illustrates Orai1 silencing efficiency. A  $65 \pm 5\%$  decrease of Orai1 expression was observed in myoblasts transfected with siOrai1 ( $n = 3$ ).

To assess the endogenous function of STIM1L, we used differentiated skeletal muscle cells (myotubes), as these cells strongly express both STIM1 variants (Fig. 1 A). To silence STIM1L, we designed three siRNAs that targeted sequences specific to the new spliced fragment of exon 11. As shown in Fig. 3 E, the three siRNAs efficiently silenced STIM1L ( $90 \pm 6$ ,  $91 \pm 7$ , and  $91 \pm 5\%$  inhibition for siSTIM1L-1, -2, and -3, respectively) without significantly affecting STIM1S. Fig. 3 F illustrates that Tg-induced SOCE amplitude was reduced by  $56 \pm 9\%$  in STIM1L-silenced myotubes ( $n = 4$  and  $P < 0.003$ ; siSTIM1L-1 was used in this and all following experiments).

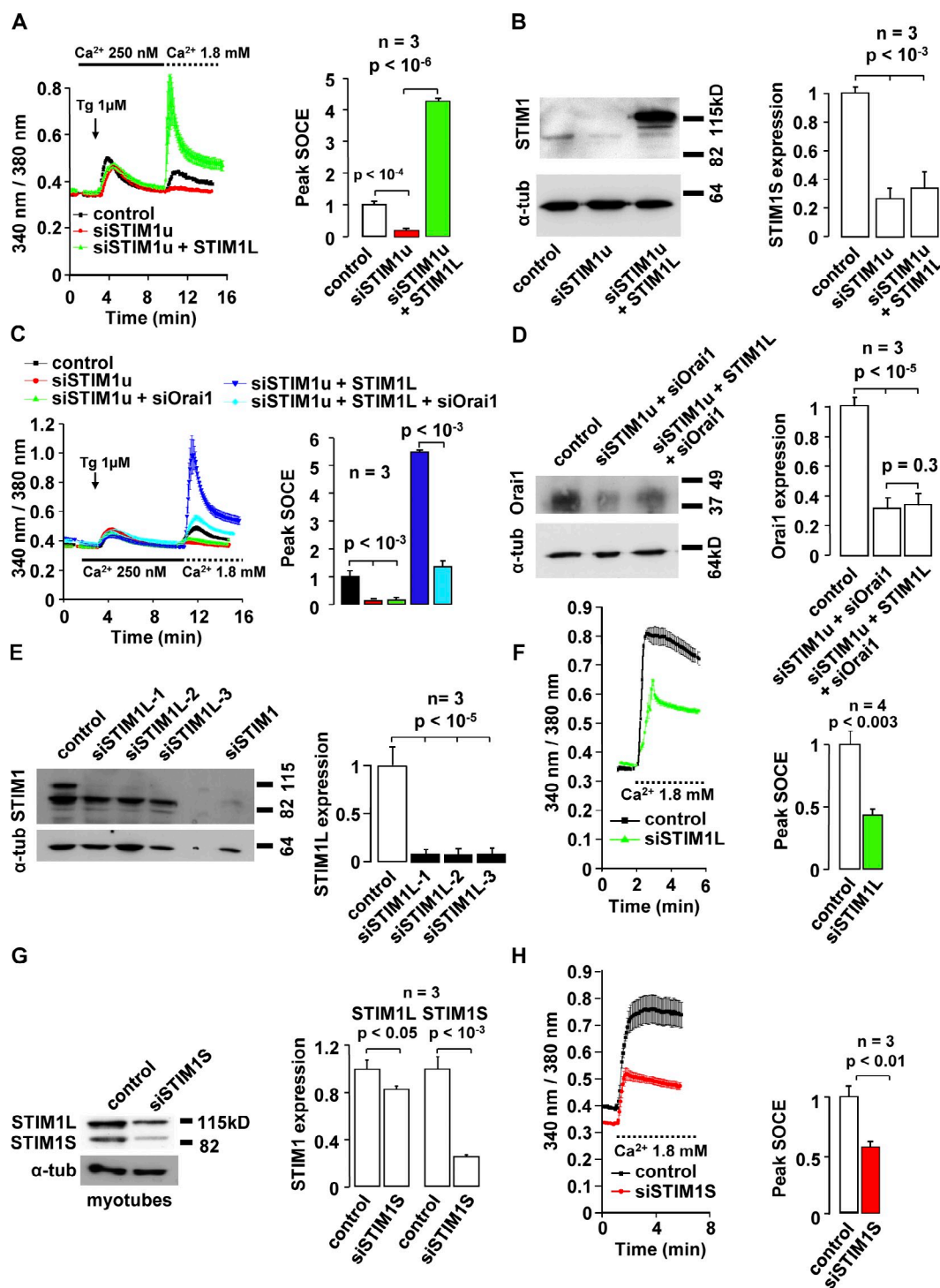


**Figure 3. STIM1L activates Orai1 and is involved in endogenous SOCE.** (A, left) Cytoplasmic  $\text{Ca}^{2+}$  was assessed with Fura-2 in proliferating myoblasts 2 d after siRNA transfection (siSTIM1u or control siRNA) and 1 d after plasmid electroporation (STIM1L or pcDNA3). As siSTIM1u targets the 3' untranslated region of STIM1 mRNA, endogenous STIM1 was silenced, whereas STIM1L vector expression was unaffected. Intracellular  $\text{Ca}^{2+}$  stores were depleted using 1  $\mu\text{M}$  Tg in a medium containing 250 nM  $\text{Ca}^{2+}$ , and, subsequently, 1.8 mM  $\text{Ca}^{2+}$  was added to the external medium to reveal SOCE (traces represent the mean  $\pm$  SEM of 10 cells; one representative experiment out of three that were performed in three different clones). (right) Mean  $\pm$  SEM peak SOCE amplitude out of three experiments. Results were normalized to control peak SOCE. (B, left) STIM1 protein expression. The same myoblasts were used for the Western blot shown and for the cytoplasmic  $\text{Ca}^{2+}$  recordings illustrated in A. (right) Mean  $\pm$  SD of three experiments. Results were normalized to control STIM1 expression and corrected for loading differences using  $\alpha$ -tubulin ( $\alpha$ -tub). (C) Same protocol as in A, except that STIM1L-YFP was used instead of STIM1L vector and EGFPN3 instead of pcDNA3 (control plasmid). Error bars represent mean  $\pm$  SEM. (D) Orai1 protein expression. The same myoblasts were used for the Western blot shown and for the cytoplasmic  $\text{Ca}^{2+}$  recordings illustrated in C. (right) Mean  $\pm$  SD of three experiments. Results were normalized to control Orai1 expression and corrected for loading differences using  $\alpha$ -tubulin. Orai1 silencing efficiency was similar in myoblasts expressing either EGFPN3 control plasmid or STIM1L-YFP plasmid (not depicted). (E, left) STIM1 expression in myotubes 96 h in differentiation medium and transfected with siRNAs (siSTIM1L1, -2, and -3) that target STIM1L-specific sequences. (right) Mean  $\pm$  SD of STIM1L expression out of three experiments. Results were normalized to STIM1L control expression and corrected for loading differences using  $\alpha$ -tubulin. (F, left) Cytoplasmic  $\text{Ca}^{2+}$  assessed with Fura-2 in myotubes



To specifically silence STIM1S, we designed and tested three siRNAs that overlapped the junction between exon 11 and 12 of STIM1S mRNA. As this sequence is absent in STIM1L mRNA, these siRNAs should silence STIM1S without modifying STIM1L expression. Two siRNAs silenced STIM1S efficiently ( $73 \pm 5$  and  $66 \pm 4\%$  inhibition for siSTIM1S-1 and -2, respectively), whereas one had no effect. STIM1L expression was only slightly reduced ( $17 \pm 3$  and  $19 \pm 4\%$  inhibition for siSTIM1S-1 and siSTIM1S-2, respectively) by both siRNAs that were efficiently silencing STIM1S. Fig. 3 (G and H) illustrates the effects of siSTIM1S-1 (the siSTIM1S that was used in all subsequent experiments) on STIM1S expression and on Tg-induced SOCE. SOCE was reduced by  $47 \pm 12\%$  in STIM1S-silenced myotubes. Note that, as formerly described, STIM1 was silenced without impeding differentiation by triggering myoblast differentiation immediately after siSTIM1S transfection (Darbellay et al., 2009, 2010). As the degree of store depletion may determine the amplitude of SOCE, we compared maximum amplitude (and also time to peak) of myoplasmic  $\text{Ca}^{2+}$  increases upon Tg addition in all conditions described in Fig. 3. No statistical difference was noted between the various conditions. Lastly, being able to specifically silence STIM1S allowed us to confirm that endogenous Orai1 is the main partner of endogenous STIM1L (Fig. S3 A).

#### Repetitive $\text{Ca}^{2+}$ releases rely on the immediate activation of the SOCE triggered by STIM1L

Experiments described in Fig. 3 (F and H) show that STIM1L and STIM1S contributions to Tg-induced SOCE amplitude were similar. As muscle cells are known to perform high frequency, high amplitude, and high duration cytosolic  $\text{Ca}^{2+}$  increases relying on release from the internal stores (Miledi et al., 1977, 1982; Gorassini et al., 2000), we compared the respective role of STIM1L and STIM1S during repetitive  $\text{Ca}^{2+}$  releases in myotubes. To simulate the excitation/contraction coupling mechanism normally occurring during skeletal muscle contraction, we increased the  $\text{K}^+$  concentration of the superfusion solution (Stiber et al., 2008; Darbellay et al., 2010). Each extracellular 65-mM KCl pulse generated large cytosolic  $\text{Ca}^{2+}$  transients that were visualized with Fura-2. Fig. 4 A illustrates that control myotubes exposed to seven consecutive pulses of 65 mM KCl were able, after an initial decrement, to perform six similar cytosolic  $\text{Ca}^{2+}$  peaks. In contrast, STIM1L-silenced myotubes were unable to sustain successive  $\text{Ca}^{2+}$  peaks (Fig. 4, B and D). After the seven KCl pulses, internal  $\text{Ca}^{2+}$  store content was assessed using 2  $\mu\text{M}$  Tg and 10 mM caffeine in 250 nM of external  $\text{Ca}^{2+}$ . Compared with control myotubes (Fig. 4 A),  $\text{Ca}^{2+}$  store content was reduced by  $87 \pm 6\%$  in STIM1L-silenced

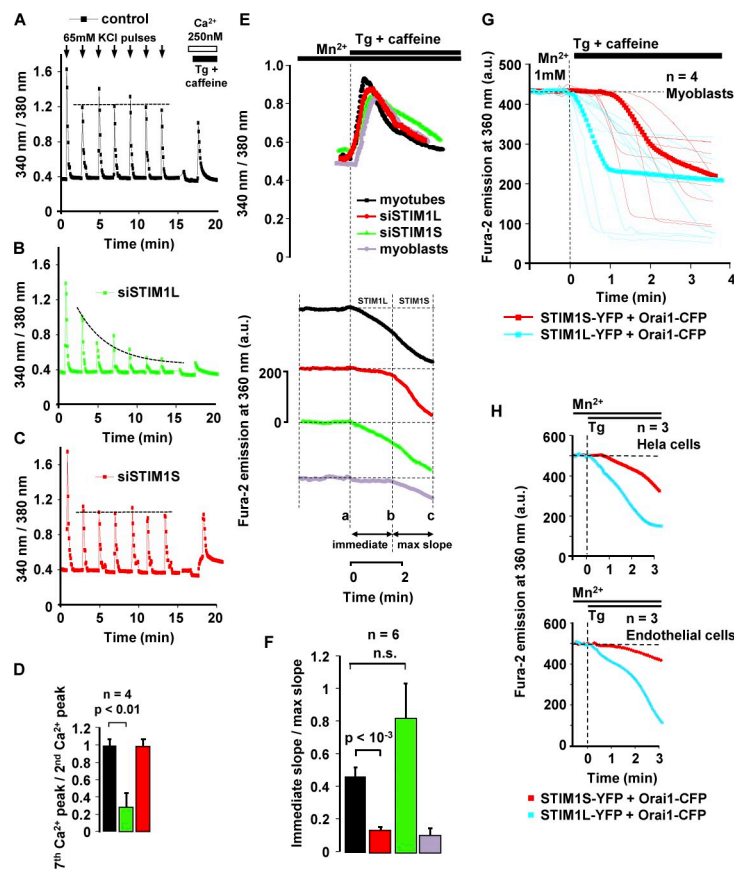
myotubes ( $P < 10^{-3}$ ; Fig. 4 B). Finally, STIM1S silencing inhibited neither KCl-induced  $\text{Ca}^{2+}$  releases nor  $\text{Ca}^{2+}$  store content, although the mean  $\text{Ca}^{2+}$  peak in STIM1S-silenced myotubes was slightly reduced (Fura-2 ratio was  $1.05 \pm 0.05$  in STIM1S-silenced myotubes vs.  $1.23 \pm 0.09$  in control myotubes;  $P < 10^{-3}$ ; Fig. 4, C and D). From these results, we concluded that STIM1S-dependent SOCE is too slow to compensate for the  $\text{Ca}^{2+}$  extrusion occurring during repetitive cytosolic  $\text{Ca}^{2+}$  increases. Indeed, in the absence of STIM1L, few releases lasting 15 s were sufficient to totally empty internal  $\text{Ca}^{2+}$  stores.

To test whether STIM1L could be responsible for a rapid SOCE activation that would without delay compensate  $\text{Ca}^{2+}$  extrusion, the onset of SOCE was evaluated by assessing  $\text{Mn}^{2+}$  quench of Fura-2 (Hoth and Penner, 1992; Fasolato et al., 1993).  $\text{Mn}^{2+}$  enters cells through  $\text{Ca}^{2+}$  channels and quenches Fura-2 fluorescence. The decrease of Fura-2 emission at 360 nm is thus directly linked to the  $\text{Ca}^{2+}$  influx. Fig. 4 E (top) illustrates ER  $\text{Ca}^{2+}$  release triggered by Tg and caffeine in the presence of 0.5 mM  $\text{Mn}^{2+}$ . Fig. 4 E (bottom) represents, in the same cells, Fura-2 quench by  $\text{Mn}^{2+}$  entering through  $\text{Ca}^{2+}$  channels activated by the ER depletion. As shown, in the presence of STIM1L (myotubes), Fura-2 emission at 360 nm strongly decreased immediately after Tg and caffeine addition, whereas in the absence of STIM1L (myoblasts), a similar decrease occurred but was delayed by  $\sim 2$  min. In addition,  $\text{Ca}^{2+}$  influx activation was also delayed in STIM1L-silenced myotubes (Fig. 4 E, red curve). However, this delay did not occur in STIM1S-silenced myotubes (Fig. 4 E, green curve).

The bar graph (Fig. 4 F) illustrates that, in the presence of STIM1L (control myotubes),  $47 \pm 6\%$  of the maximum slope of the Fura-2 quench trace was induced immediately after store depletion, whereas this fraction dropped to  $14 \pm 2\%$  in STIM1L-silenced myotubes (STIM1S present only) and to  $11 \pm 5\%$  in control myoblasts (STIM1S present only). As expected, in STIM1S-silenced myotubes (STIM1L present only), the fraction of the maximum slope induced immediately was large ( $83 \pm 21\%$ ). Fig. S3 B shows that double silencing of STIM1L and STIM1S totally inhibited the influx triggered by the Tg and caffeine, confirming that this influx was purely STIM1 dependent. Results from experiments in which STIM1L is exogenously expressed in three cell types that do not have endogenous STIM1L are in full agreement with the previous findings (shown in Fig. 4, E and F). Fig. 4 (G and H) illustrates that exogenous STIM1L-YFP expression in myoblasts, a human umbilical vein endothelial cell-derived cell line (EA.hy926), and HeLa cells allows immediate SOCE activation after Tg. These results have to be compared with STIM1S-YFP expression that, in the same cells, does not allow immediate SOCE activation. Fluorescence resonance energy transfer (FRET) increase between STIM1S-CFP

96 h after siRNA transfection and differentiation induction. SOCE was evaluated as in A. Traces represent the mean  $\pm$  SEM of three multinucleated myotubes (black and green traces). One representative experiment out of four that were performed in three different clones (15 myotubes were assessed in each condition). (right) Mean  $\pm$  SD peak SOCE amplitudes normalized to control myotubes ( $n = 4$  experiments). (G, left) STIM1 expression in control and siSTIM1S-transfected myotubes at 96 h in differentiation medium. (right) Western blot quantifications (mean  $\pm$  SD of three experiments in three different clones). Results were normalized to STIM1L and -S control expression and corrected for loading differences using  $\alpha$ -tubulin. (H, left) Tg-induced SOCE measured with Fura-2 in myotubes at 96 h in differentiation medium and transfected with siSTIM1S or control siRNA (same protocol as in C; mean  $\pm$  SEM of 10 myotubes). (right) Mean  $\pm$  SD peak SOCE amplitudes out of three experiments. Results were normalized to control SOCE amplitude.

**Figure 4. Repetitive  $\text{Ca}^{2+}$  signals encoded by  $\text{Ca}^{2+}$  release rely on STIM1L.** (A–C)  $\text{Ca}^{2+}$  transients induced by seven 65-mM KCl pulses and evaluated with Fura-2 in control (A), transfected siSTIM1L (B), and transfected siSTIM1S (C) myotubes at 96 h in differentiation medium.  $\text{Ca}^{2+}$  store content was then assessed using 2  $\mu\text{M}$  Tg and 10 mM caffeine in 250 nM of external  $\text{Ca}^{2+}$  medium. Each trace represents the mean of 10 recorded cells. In A and C, the horizontal dotted line represents the mean  $\text{Ca}^{2+}$  peak (the first peak was excluded), and, in B, the dotted line is an exponential fit through  $\text{Ca}^{2+}$  peaks (the first peak was excluded). (D) Amplitude of the second KCl-induced  $\text{Ca}^{2+}$  peak divided by the amplitude of the seventh KCl-induced  $\text{Ca}^{2+}$  peak (mean  $\pm$  SD; 10 cells out of four experiments in each condition). (E, top) Cytoplasmic  $\text{Ca}^{2+}$  assessed with Fura-2 in myoblasts and in myotubes 48 h after transfections with various siSTIM1.  $\text{Ca}^{2+}$  stores were depleted with 10 mM caffeine and 2  $\mu\text{M}$  Tg in 1.8 mM of external  $\text{Ca}^{2+}$  and 0.5 mM of external  $\text{Mn}^{2+}$ . (bottom) Fura-2 fluorescence at a 360-nm excitation. Cytoplasmic  $\text{Ca}^{2+}$  and Fura-2 fluorescence quench were measured simultaneously. No statistical difference was noted between maximum amplitude (and also time to peak) of myoplasmic  $\text{Ca}^{2+}$  increases upon Tg/caffeine addition. a.u., arbitrary unit. (F) Fraction of the maximum slope of Fura-2 quench traces that occurred immediately after  $\text{Ca}^{2+}$  store depletion with 2  $\mu\text{M}$  Tg and 10 mM caffeine. Immediate activation slopes were measured between times a and b and maximum slopes between times b and c in E. Mean  $\pm$  SEM of six experiments using 0.5–1 mM  $\text{Mn}^{2+}$  (13 cells were recorded in each experiment; also see Fig. S3 B). (G and H) Fura-2 fluorescence quench at 360 nm measured in myoblasts, HeLa cells, and EA.hy926 (human endothelial) cells with 1 mM  $\text{Mn}^{2+}$  in the external medium. For HeLa and EA.hy926 cells,  $\text{Ca}^{2+}$  stores were depleted with 2  $\mu\text{M}$  Tg in 1.8 mM of external  $\text{Ca}^{2+}$ . The squares represent the mean of six to eight cells out of three to four experiments. The thin lines represent individual cell traces. n.s., not significant. The vertical and horizontal dashed lines represent the application of Tg ( $\pm$  caffeine) at time 0 and initial Fura-2 fluorescence at 360 nm, respectively.



and -YFP after stimulation with 2  $\mu\text{M}$  Tg and 10 mM caffeine had a  $t_{1/2}$  of  $20 \pm 3$  s (Fig. S3 C), which excludes that the delay of SOCE activation in STIM1S-expressing cells was caused by a slow action of Tg and caffeine. From these results, we conclude that fast SOCE activation in myotubes depends on STIM1L expression and that fast SOCE activation is required to perform repetitive store-dependent  $\text{Ca}^{2+}$  signals.

### STIM1L interacts with actin to form permanent clusters

The delay that characterized the activation of the STIM1S-dependent SOCE is linked to the process of STIM1S migration and cluster formation that precedes the activation of Orail channels (Liou et al., 2007). We thus wondered whether STIM1L clusters could form faster (or using a different mechanism) than STIM1S clusters. To examine this hypothesis, we overexpressed STIM1L- and STIM1S-YFP into myoblasts and compared their cellular distribution before and after Tg-induced store depletion. As expected, STIM1S was diffusely distributed in resting myoblasts with filled  $\text{Ca}^{2+}$  stores, and clusters formed within 2–4 min after  $\text{Ca}^{2+}$  store depletion (Fig. 5 A, left). What was not expected, however, was that STIM1L clusters were already fully formed in resting myoblasts (with filled  $\text{Ca}^{2+}$  stores) and that their distribution did not change after Tg exposure (Fig. 5 A, right). Interestingly, STIM1L clusters were distributed along parallel lines in both conditions. Similar results were obtained with human endothelial cells overexpressing YFP-tagged STIM1S or STIM1L (unpublished data), suggesting that these

observations are directly related to STIM1L properties and not to the cell type in which STIM1L is expressed.

The next step was to evaluate whether the STIM1L additional sequence is involved in cluster preformation and alignment. For that purpose, we cloned the last two exons of STIM1L and STIM1S (exons 11 and 12), tagged them with GFP, and overexpressed them in myoblasts. Fig. 5 C shows that GFP-tagged STIM1S exons 11 and 12 were uniformly distributed, and neither puncta nor linear structures were ever observed, whereas GFP-tagged STIM1L exons 11 and 12 formed linear clusters in all observed cells ( $>100$  cells in eight experiments). The level of  $\text{Ca}^{2+}$  in stores had no influence on these results, as these small constructs lack the  $\text{Ca}^{2+}$  sensor (unpublished data). Fig. S4 (A and B) shows that GFP-tagged exons 11 and 12 of both STIM1L and STIM1S can be expressed in myoblasts and that these fragments have a dominant-negative effect on Tg-induced SOCE amplitude.

As STIM1L forms linear clusters, we assessed a possible involvement of actin filaments in the anchoring and permanent clustering of STIM1L. Figs. 5 C and S4 C show that STIM1L exons 11 and 12–GFP and STIM1L-GFP formed linear clusters that perfectly colocalized with actin filaments in unstimulated myoblasts. In contrast, STIM1S clusters did not colocalize with actin filaments (Fig. 5 D). The distinct patterns of Fig. 5 (C and D) suggest that STIM1S and STIM1L clusters did not colocalize after store depletion. However, overexpression of STIM1S-mCherry and STIM1L-GFP in the same cells shows a little overlap of STIM1S/L clusters, suggesting that a fraction of

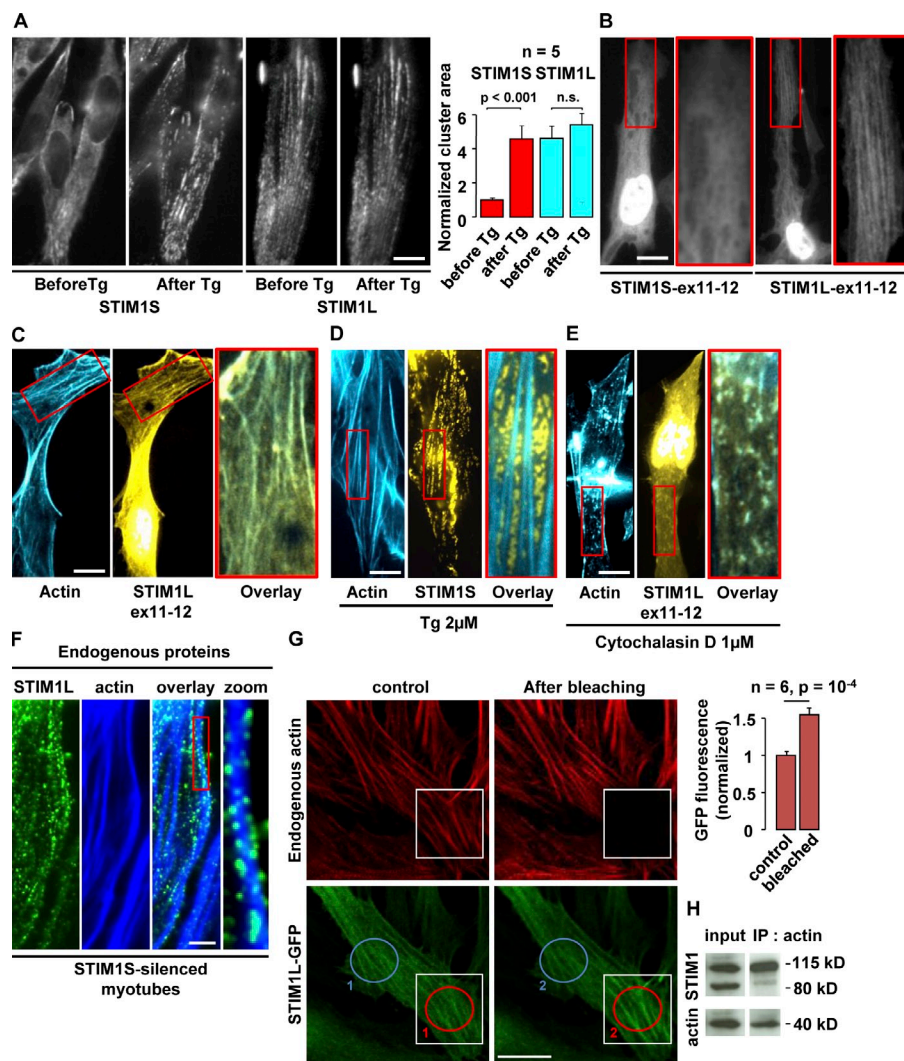


**Figure 5. STIM1L interacts with actin and forms permanent clusters that colocalize with Orai1 in store-filled cells.** (A) Distribution of STIM1S-YFP and STIM1L-YFP overexpressed in myoblasts before and after treatment with 2  $\mu$ M Tg. The bar graph represents the total surface area of clusters in the various conditions. Clusters were detected with an automatic detection of fluorescence intensity variations called “by edges” (mean  $\pm$  SD and  $n = 5$  experiments; MetaMorph 7.5.6; Molecular Devices). Bar, 20  $\mu$ m. (B) Distribution of STIM1S exons 11 and 12-GFP and STIM1L exons 11 and 12-GFP in store-emptied cells using 2  $\mu$ M Tg. Red rectangles show enlarged images. Bar, 20  $\mu$ m. (C–E) Distribution and colocalization of actin (detected by phalloidin-TRITC) and STIM1L exons 11 and 12-GFP (C), distribution of actin (detected by phalloidin-TRITC) and STIM1S-YFP 5 min after treatment with 2  $\mu$ M Tg (D), and distribution of actin (detected by phalloidin-TRITC) and STIM1L exons 11 and 12-GFP in myoblasts treated with 1  $\mu$ M cytochalasin D for 3 h at room temperature (E). Bars, 20  $\mu$ m. (F) Distribution of endogenous STIM1L (detected with an antibody against both STIM1 isoforms) and actin (detected by phalloidin-Atto 390) in STIM1S-silenced myotubes. Bar, 5  $\mu$ m. (G) Acceptor photobleaching method to measure FRET between actin (detected by phalloidin-TRITC) and STIM1L-GFP in fixed myoblasts 24 h after electroporation. The blue and red circles indicate regions used for GFP fluorescence measurements, and white squares indicate 561-nm bleached regions. The bar graph illustrates the mean  $\pm$  SD of GFP fluorescence increases when acceptor (actin-phalloidin-TRITC) is bleached. Measurements were normalized to GFP fluorescence variation in control regions (fluorescence ratio of red regions [2:1] was divided by the fluorescence ratio of blue regions [2:1]). Bar, 10  $\mu$ m. (H) Western blot illustrating coimmunoprecipitation (IP) of endogenous STIM1L using an antibody against actin. One representative experiment out of three. All images are shown in pseudocolors.

STIM1S may be recruited in STIM1L clusters after store depletion (unpublished data). Treatment with 1  $\mu$ M cytochalasin D (3 h at room temperature) largely disrupted the actin organization in 60% of the myoblasts, and, in these cells, the linear organization of STIM1L exons 11 and 12-GFP disappeared, although STIM1L exons 11 and 12-GFP and disrupted fragments of actin still colocalized perfectly (Fig. 5 E). A similar result was obtained in STIM1L-expressing cells using either 1  $\mu$ M cytochalasin D or 1  $\mu$ M latrunculin B, and a partial effect was obtained using 0.1 and 0.5  $\mu$ M cytochalasin D (Figs. S4 C and S5 A). We also verified that STIM1S clusters still formed and remained stable in actin-disrupted cells after Tg-induced  $\text{Ca}^{2+}$  store depletion (unpublished data). As shown in Fig. 5 F, endogenous STIM1L also forms linear clusters that colocalize with actin in STIM1S-silenced myotubes. In addition, Fig. 5 G shows that FRET occurs between phalloidin-TRITC-labeled actin and STIM1L-GFP, further suggesting a close vicinity (within  $\sim 10$  nm) between these two molecules. Finally, Fig. 5 H shows the coimmunoprecipitation of STIM1L but not STIM1S using an actin antibody.  $87 \pm 6\%$  of the input amount of endogenous

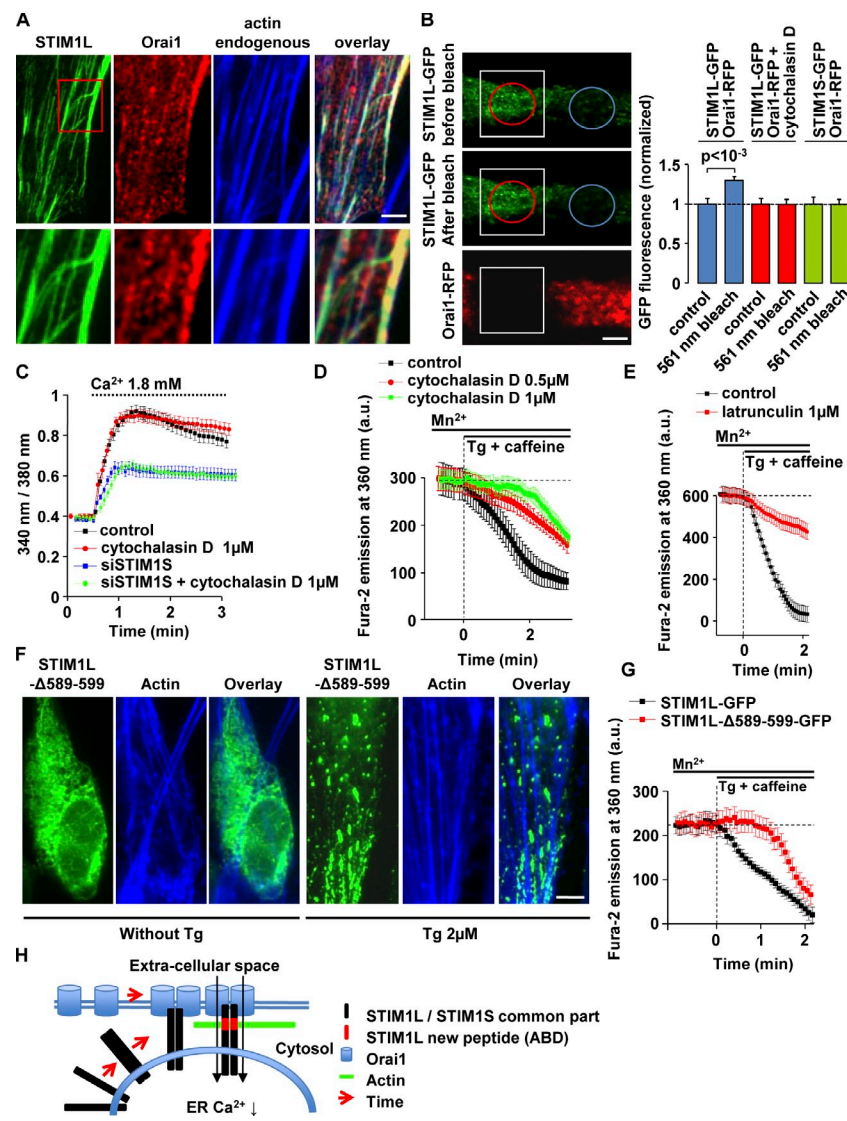
STIM1L proteins was immunoprecipitated by actin ( $P = 0.009$ ), whereas only  $6 \pm 4\%$  of endogenous STIM1S was detected. Altogether, these results strongly suggest that actin fibers are involved in STIM1L cluster preformation in store-filled cells through a very close interaction between STIM1L and actin.

#### Actin fiber disruption dissociates STIM1L-Orai1 preformed complexes and delays SOCE activation

We first verified that STIM1L clusters (present when  $\text{Ca}^{2+}$  stores are filled) colocalized with Orai1 clusters, as this partner is required for SOCE activation. To assess this point, we simultaneously overexpressed Orai1-RFP and STIM1L-YFP in myoblasts. Fig. 6 A illustrates that Orai1 forms linear clusters in resting cells and that these clusters colocalize with STIM1L clusters. Fig. 6 A also shows that, as expected, linear clusters of STIM1L and Orai1 colocalize with actin fibers (detected with phalloidin-Atto 390). On the other hand, Fig. S5 B illustrates that neither Orai1-RFP nor STIM1S-GFP formed clusters in myoblasts with filled  $\text{Ca}^{2+}$  stores. FRET measurements between STIM1L-GFP and Orai1-RFP confirm that



**Figure 6. Actin fiber disruption dissociates STIM1–Orai1 preformed complexes and delays SOCE activation.** (A) Distribution and colocalization of STIM1L-GFP, Orai1-RFP, and actin in resting myoblasts (filled  $\text{Ca}^{2+}$  stores). Actin was detected with phalloidin–Atto 390. One representative cell out of >30 cells in three experiments. The red box outlines the enlarged image shown on the bottom. Bar, 5  $\mu\text{m}$ . (B) Acceptor photobleaching method to measure FRET between Orai1-RFP and either STIM1L- or STIM1S-GFP in fixed myoblasts 24 h after electroporation. The bar graph shows the mean  $\pm$  SD, and the horizontal dashed line represents the control FRET level. GFP fluorescence increases when acceptor (Orai1-GFP) is bleached ( $n = 8$  for each condition). Analysis was performed as described in Fig. 5 G. The blue and red circles indicate regions used for GFP fluorescence measurements, and white squares indicate 561-nm bleached regions. Bar, 5  $\mu\text{m}$ . (C) Cytoplasmic  $\text{Ca}^{2+}$  assessed with Fura-2 to evaluate maximum SOCE in control and STIM1S-silenced myotubes in the absence or presence of 1  $\mu\text{M}$  cytochalasin D.  $\text{Ca}^{2+}$  stores were depleted with 2  $\mu\text{M}$  Tg and 10 mM caffeine in 250 nM of external  $\text{Ca}^{2+}$ , and, subsequently, 1.8 mM  $\text{Ca}^{2+}$  was added to the external medium to reveal SOCE (traces represent the mean  $\pm$  SEM of 76 cells;  $n = 3$  experiments in three clones). (D) Fura-2 fluorescence quench at 360 nm measured in myotubes (with 1 mM  $\text{Mn}^{2+}$  in the external medium) in the absence or presence of 0.5 and 1  $\mu\text{M}$  cytochalasin D.  $\text{Ca}^{2+}$  stores were depleted with 2  $\mu\text{M}$  Tg and 10 mM caffeine in 1.8 mM of external  $\text{Ca}^{2+}$  (mean  $\pm$  SEM of 16 cells;  $n = 3$  experiments). (E) Same experiment as in D, except that myoblasts overexpressing STIM1L-YFP and Orai1-RFP were used instead of myotubes and that actin depolymerization was obtained using 1  $\mu\text{M}$  latrunculin instead of cytochalasin D (mean  $\pm$  SEM of 13 cells;  $n = 3$  experiments). (F) Myoblasts at 24 h after electroporation with STIM1L- $\Delta$ 589–599-GFP before and after treatment with 2  $\mu\text{M}$  Tg for 15 min (one representative experiment out of three). Bar, 5  $\mu\text{m}$ . (G) Fura-2 fluorescence quench at 360 nm measured in STIM1S-silenced myoblasts (with 1 mM  $\text{Mn}^{2+}$  in the external medium and 48 h after siSTIM1S transfection) expressing either STIM1L- $\Delta$ 589–599-GFP or STIM1L-GFP.  $\text{Ca}^{2+}$  stores were depleted with 2  $\mu\text{M}$  Tg and 10 mM caffeine in 1.8 mM of external  $\text{Ca}^{2+}$  (mean  $\pm$  SEM of 12 cells;  $n = 5$  experiments). (D, E, and G) Vertical dashed lines represent the application of Tg and caffeine at time 0, and horizontal dashed lines represent the initial Fura-2 fluorescence at 360 nm. (H) SOCE activation by STIM1L and -S. In resting (store filled) cells, STIM1L is already associated with Orai1 and forms permanent clusters via its interaction with actin filaments. Upon store depletion, STIM1L triggers SOCE without delay. STIM1S-dependent SOCE requires homomerization, migration, and cluster formation of STIM1S molecules, a process that needs  $\sim 2$  min to take place. This second process, which occurs during a long-lasting decrease of the  $\text{Ca}^{2+}$  store content, results in a global increase of SOCE amplitude. All images are shown in pseudocolors. ABD, actin-binding domain of STIM1L; a.u., arbitrary unit.



these two molecules are located in close proximity (Fig. 6 B, left images and right blue bars) and that this close proximity is disrupted by 1  $\mu\text{M}$  cytochalasin D (Fig. 6 B, red bars). The absence of FRET between STIM1S-GFP and Orai1-RFP in store-filled myoblasts was assessed as a control (Fig. 6 B, green bars).

Finally, we assessed the impact on SOCE of actin disruption and transfection of an STIM1L mutant missing amino acids 589–599 (STIM1L- $\Delta$ 589–599-GFP), a mutant that did not form permanent clusters in store-filled cells. Fig. 6 C shows that actin disruption with 1  $\mu\text{M}$  cytochalasin D had no effect on endogenous maximal SOCE amplitude in normal or STIM1S-silenced myotubes. This result suggests that neither STIM1L nor STIM1S relies on actin integrity to control maximal SOCE amplitude. However, and as expected, endogenous SOCE activation was clearly delayed in myotubes after actin depolymerization with 1 and 0.5  $\mu\text{M}$  cytochalasin D (Fig. 6 D). Accordingly, the acceleration of

SOCE activation conferred by STIM1L overexpression in myoblasts (Fig. 4 G) was reversed by actin disruption (Fig. 6 E). Fig. 6 F shows the distribution in myoblasts of STIM1L- $\Delta$ 589–599-GFP, a mutant missing an amino acid sequence located within the actin-binding domain. Neither clusters nor lines were observed in store-filled myoblasts transfected with this mutant. Fig. 6 F also shows that, although store depletion with Tg still induced cluster formation, these clusters did not colocalize with actin fibers. Lastly, Fig. 6 G illustrates that  $\text{Mn}^{2+}$  quench of the Fura-2 fluorescence was severely delayed in STIM1S-silenced myoblasts expressing STIM1L- $\Delta$ 589–599-GFP, an expected result in the absence of permanent STIM1L clusters in store-filled cells. From these results, we conclude that actin fibers stabilize inactivated STIM1L–Orai1 complexes in naive store-filled cells and, by this mechanism, allow fast SOCE activation upon  $\text{Ca}^{2+}$  store depletion in STIM1L-expressing cells.



## Discussion

Here, we identified a longer form of the STIM1 protein, STIM1L, which allows immediate activation of SOCE and is required to trigger repetitive cytosolic  $\text{Ca}^{2+}$  releases. STIM1L is the product of an alternative splicing on exon 11 of the STIM1 gene and is expressed in many mammalian tissues. Live cell imaging showed that STIM1L–Orai1 clusters were already present at rest when  $\text{Ca}^{2+}$  stores were full. In contrast, STIM1S molecules were diffusely distributed at rest, and it took >1 min for STIM1S clusters to fully form after  $\text{Ca}^{2+}$  store depletion (Liou et al., 2007). As the main cause of the STIM1S-related SOCE activation delay appears to be the time required for STIM1S to migrate, form clusters, and bind to Orai1 (Liou et al., 2007; Navarro-Borelly et al., 2008; Calloway et al., 2009), the presence of permanent STIM1L–Orai1 clusters could explain the rapid SOCE activation in STIM1L-expressing cells. In myoblasts, STIM1S oligomerized within 10 s of Tg and caffeine application (Fig. S3 C), whereas SOCE activation was delayed >1 min (Fig. 4 G). A similar result was obtained in myotubes. These observations confirm that the delay characterizing STIM1S-related SOCE activation is a result of the overall process of STIM1S oligomerization, migration, and binding to Orai1. The kinetics of STIM1S oligomerization after store depletion (<10 s; Fig. S3 C) also suggests that a difference between STIM1S and STIM1L luminal  $\text{Ca}^{2+}$  affinity, if present, will not play a major role in the overall delay of STIM1S-dependent SOCE activation. Here, we also showed that the formation of permanent clusters is directly linked to the interaction of the added sequence of STIM1L with actin, as STIM1L–GFP, the GFP-tagged exons 11 and 12 of STIM1L, and endogenous STIM1L form linear clusters that colocalize with actin and disappear upon actin depolymerization. In addition, endogenous STIM1L was coimmunoprecipitated by actin. Finally, we observed that an STIM1L mutant missing a 10–amino acid sequence within the actin-binding domain forms clusters only after store depletion, does not colocalize with actin, and triggers slow SOCE activation. Although these last results do not prove a direct binding between the 589–599 amino acid fragment and actin, they clearly suggest that this fragment is required for the STIM1L–actin interaction to take place.

In skeletal muscle fibers, SOCE has been shown to be maximally activated in <1 s after the initiation of the  $\text{Ca}^{2+}$  store release, whereas full SOCE activation takes several seconds (up to 260 s for complete cluster formation) in other cell types (Parekh and Putney, 2005; Wu et al., 2006; Launikonis and Ríos, 2007; Liou et al., 2007; Navarro-Borelly et al., 2008; Calloway et al., 2009). We confirmed that, in human myotubes, the immediate activation of SOCE relies on endogenous STIM1L and that exogenous expression of STIM1L triggers immediate SOCE activation regardless of the cell types, linking this specific feature of SOCE to STIM1L expression. As actin depolymerization disrupts STIM1L–Orai1 resting complexes and delays SOCE activation without decreasing maximal SOCE amplitude, we conclude that STIM1L–actin interaction stabilizes preformed SOCE complexes, which in turn trigger fast SOCE activation.

In STIM1L-silenced myotubes, repetitive  $\text{Ca}^{2+}$  release with a frequency faster than the time required to activate

STIM1S-related SOCE rapidly emptied the  $\text{Ca}^{2+}$  content of the stores. Physiological muscle contractions involve repetitive bursts of tetanic stimulations that may last a few seconds (Miledi et al., 1977, 1982; Buchthal and Schmalbruch, 1980; Stein et al., 1988; Kiehn and Eken, 1997, 1998; Gorassini et al., 2000; Reklings et al., 2000). As cytosolic  $\text{Ca}^{2+}$  concentration remains elevated during most of the tetanic contraction, such a stimulation pattern produces a small but constant extrusion of  $\text{Ca}^{2+}$  in the extracellular space through the plasma membrane  $\text{Ca}^{2+}$  ATPase and  $\text{Na}^{+}$ – $\text{Ca}^{2+}$  exchanger (Cifuentes et al., 2000; Caride et al., 2001). To compensate for this  $\text{Ca}^{2+}$  efflux, SOCE or other  $\text{Ca}^{2+}$  influxes need to be activated as soon as contraction begins. We thus propose that STIM1L may be involved in the rapid SOCE activation required to compensate for the  $\text{Ca}^{2+}$  efflux occurring during normal muscle contraction (Stiber et al., 2008). This model would explain well why skeletal muscle contraction requires functional SOCE (Kurebayashi and Ogawa, 2001; Zhao et al., 2005; Ducret et al., 2006; Lyfenko and Dirksen, 2008; Stiber et al., 2008; Dirksen, 2009; Darbellay et al., 2010; Edwards et al., 2010; Launikonis et al., 2010), even though SOCE amplitude would appear, a priori, as insufficient to significantly contribute to  $\text{Ca}^{2+}$  store refilling when compared with  $\text{Ca}^{2+}$  recycling by the sarco/ER  $\text{Ca}^{2+}$  ATPase. It would further explain why, in *Stim1*<sup>+/–</sup> knockout mice, muscle weakness is only revealed during tetanic stimulations, whereas single-twitch contractions are normal (Stiber et al., 2008).

Based on the findings in the present and former studies (Miledi et al., 1982; Launikonis and Ríos, 2007; Stiber et al., 2008; Feske, 2009; Launikonis et al., 2009; McCarl et al., 2009; Darbellay et al., 2010; Edwards et al., 2010), we propose the model summarized in Fig. 6. The presence of a new STIM isoform, STIM1L, able to permanently cluster STIM1 molecules and thus activate SOCE immediately after store depletion, would allow any cell type to perform repetitive cytosolic  $\text{Ca}^{2+}$  releases with frequencies in seconds or faster.

## Materials and methods

### Cell culture

Muscle samples, cell dissociation, and clonal culture from satellite cells were prepared as previously described (Baroffio et al., 1993; Arnaudeau et al., 2006). In brief, muscle biopsies were minced and incubated for 1 h in a solution containing 0.5 mg/ml<sup>–1</sup> trypsin. The suspension was centrifuged and resuspended several times in a wash medium to remove muscular debris (Ham's F10 with 15% FCS). Red blood cells were lysed with Tris–ammonium chloride buffer. Using a micropipette, single satellite cells were then manually collected (clonal culture). Human muscle samples were obtained from eight children (operated for clubfoot and <4 yr old) without any known neuromuscular disease. Plasmids (Orai1-RFP was provided by D. Al-Ansary and B. Niemeyer, Saarland University, Homburg, Germany; STIM1-YFP [19754; Addgene; Prakriya et al., 2006], STIM1S-mCherry, STIM1L, STIM1L-YFP, STIM1S–C terminal, and STIM1L–C terminal) were transfected by electroporation with a Nucleofector II device (Lonza). Following the manufacturer's protocol, a suspension of  $5 \times 10^5$  myoblasts, HeLa cells, or endothelial cells (provided by C.J.S. Edgell, University of North Carolina at Chapel Hill, Chapel Hill, NC) and 2  $\mu\text{g}$  plasmid DNA and/or 0.1–0.2 nM siRNA was electroporated. The transfection efficiency assessed by FACS was >80% for tagged plasmids.

### siRNA knockdown

Myoblasts were transfected in suspension by incubating  $4 \times 10^5$  cells in a solution containing 500  $\mu\text{l}$  Opti-MEM, 3  $\mu\text{l}$  Lipofectamine RNAiMax (Invitrogen), and 20 pmol of a specific siRNA (Invitrogen)

according to manufacturer protocols (Invitrogen). The transfection efficiency assessed by Alexa Fluor red fluorescent oligonucleotide (Block-iT; Invitrogen) measurements was ~90%. Three different siSTIM1 siRNAs (Invitrogen) targeting the longer STIM1 isoform (STIM1L) were used (sense strand siRNA): siSTIM1L-1 5'-GCCGGGUAUCUCUGCGGCGT-3', siSTIM1L-2 5'-UGCGCAGCCUUUCUACUGGTT-3', and siSTIM1L-3 5'-GGCUACGGGACCAGCUCUCh-3'.

These different siRNAs gave similar results on protein amount silencing analyzed by Western blots. To simplify, all results shown in this study were obtained with siSTIM1L-1. STIM1 and Orai1 siRNAs were previously described as siSTIM1<sub>a</sub> (siSTIM1 in this study), siSTIM1<sub>b</sub> (targeting the 3' untranslated noncoding region of the STIM1 mRNA and called siSTIM1<sub>u</sub> in this study), and siOrai1<sub>b</sub> (Darbellay et al., 2009). Two different siSTIM1 siRNAs (Invitrogen) targeting the shorter STIM1 isoform (STIM1S) were used (sense strand siRNA): siSTIM1S-1 5'-GGGAUCUCAGAGGGAUUGGTT-3' and siSTIM1S-2 5'-CAGAGGGAUUGACCAUUT-3'.

siSTIM1S-1 and siSTIM1S-2 give similar results on STIM1S amount on Western blots. To simplify, all results shown in this study were obtained with siSTIM1S-1. The siRNA siMed negative control (Invitrogen) was used as a control.

### Western blots and immunoprecipitations

Western blots were performed as previously described (Konig et al., 2004). In brief, myoblasts were lysed using NP-40 extraction buffer (Invitrogen). Total proteins were separated on an SDS-PAGE and transferred to nitrocellulose membranes. Membranes were incubated in TBS (0.1% Tween 20, 20 mM Tris-HCl, pH 7.5, and 137 mM NaCl) and 5% nonfat milk. Blots were incubated overnight with the following primary antibodies diluted in TBS and nonfat milk: mouse monoclonal antibody anti-GOK/STIM1 (1:500; BD), rabbit antibodies anti-STIM1 (1:2,000, N and C terminal; Sigma-Aldrich), rabbit polyclonal anti-Orai1 (1:1,000; Proscil), mouse monoclonal antibody anti- $\alpha$ -tubulin (1:10,000, clone DM1A; Sigma-Aldrich), and mouse monoclonal antiactin (1:50,000, clone C4; Millipore). Blots were incubated for 1 h with HRP-conjugated goat anti-mouse or -rabbit diluted antibodies (1:6,000; Bio-Rad Laboratories). Antibodies were revealed using Plus-ECL reagents (PerkinElmer) and Hyperfilm ECL (GE Healthcare). Optiquant 03.00 software (Packard Instrument Company) was used to quantify the level of protein expression.  $\alpha$ -Tubulin is shown as a loading control. Protein extracts from severe combined immunodeficiency mice were used to assess STIM1 expression in various organs. Actin immunoprecipitation was performed using approximately two million differentiated myoblasts in NP-40 buffer. Samples were precleared with protein G beads. Cells were incubated overnight with antiactin antibody and protein G beads. Precipitate was then washed with buffer before performing the Western blots. T cells were provided by J.M.R. Garriz (Geneva University Hospital, Geneva, Switzerland).

### Cytosolic calcium measurements and fluorescence imaging

Myoblasts grown on coverslips were loaded 30 min at room temperature with the cell-permeant fluorescent  $\text{Ca}^{2+}$  indicator Fura-2-acetoxymethyl (AM; Biotium, Inc.). Fura-2-AM preparation was performed as previously described (Arnaudeau et al., 2006). In brief, Fura-2-AM was diluted in medium to a final concentration of 2  $\mu\text{M}$  from a DMSO stock solution containing 1 mM Fura-2-AM, 100 mg/ml Pluronic F127 (Invitrogen), and 0.1% acetic acid. Ratiometric images of Fura-2 fluorescence were monitored using an Axiovert microscope (S100 TV; Carl Zeiss) equipped with a monochromator (Optoscan; Cairn Research Limited), which rapidly changed the excitation wavelengths between 340 and 380 nm. Fluorescence emissions were captured through a filter (510WB40; Omega Optical, Inc.) using a digital camera (CoolSnap HQ; Photometrics). Image acquisition and ratio analysis were performed using Metafluor software (6.3r7; Molecular Devices). The maximal ratio was evaluated in all conditions (using a solution containing 4  $\mu\text{M}$  ionomycin and 5 mM  $\text{Ca}^{2+}$ ), ruling out any possible nonlinearity between data obtained in myoblasts transfected with different plasmids or siRNA. No significant difference between the various maximal ratios was found. No significant differences between the level of expression of YFP, GFP, and RFP fluorescence intensities were noted. As tags were fused to STIMs or Orai, discrepancies between the levels of expression of the proteins were excluded. Actin was detected using phalloidin-TRITC (Millipore) and phalloidin-Atto 390 (Sigma-Aldrich).

### Confocal FRET measurements

Confocal image acquisition of FRET between STIM1L-GFP (or STIM1S-GFP) and Orai1-RFP (or phalloidin-TRITC; Millipore) was performed on fixed cells using a confocal microscope (Eclipse Ti-A1r; Nikon) with a 100 $\times$  Plan Apochromat violet-corrected 1.4 NA with a working distance of 0.13 mm.

Ratios of transfected plasmids (GFP/RFP) were 1:2. Wavelengths of the excitation laser beam were 488 and 561 nm. Images were acquired and analyzed using Nikon software.

### Cloning

Total RNA from  $2 \times 10^6$  myoblasts was extracted using TRIZOL reagent (Invitrogen). In brief, chloroform was added to the TRIZOL, extracts were centrifuged to eliminate the phenol-chloroform solution, and the aqueous part was purified. Isopropanol was then added to the aqueous part to precipitate RNA. Precipitates were washed with 75% ethanol and finally resuspended in 20  $\mu\text{l}$  diethylpyrocarbonate water. RACE was performed on 5  $\mu\text{g}$  of total RNA (Gene Racer kit; Invitrogen). In brief, after RNA dephosphorylation, decapping, and 5' oligonucleotide ligation, reverse transcription was performed using 200 U Superscript III reverse transcriptase (Invitrogen) according to the manufacturer's protocol. We amplified by PCR the cDNA ends using Platinum Taq DNA Polymerase (Invitrogen) and the following primer couples: 5' ends, GeneRacer 5' and exon 9 reverse 5'-GGAAGGTGCCAAAGAGTGTG-3', and 3' ends, GeneRacer 3', and exon 6 forward 5'-CATGCTGGTGGTGTCTATCG-3'.

Products were further amplified by nested PCR using exon 7 reverse 5'-TCCGCTCATTCTCAGTACCC-3' and exon 7 forward 5'-GCGG-GAGGGTACTGAGAATG-3' for amplification of 5' RACE and 3' RACE products, respectively. The different PCR products obtained were cloned in the TOPO TA cloning kit (Invitrogen) for sequencing.

We cloned both full-length STIM1S and -L cDNA by PCR on reverse-transcribed mRNA from myotubes using the following primer couples: STIM1-533F, 5'-TCCACATCAGACGCATGTG-3', and STIM1-2713R, 5'-GGCCAGTTATCTGAAGGAAGG-3'. Expression vectors encoding STIM1S and -L were obtained by cloning the full-length PCR products into the pcDNA 3.3-TOPO TA vector using the pcDNA 3.3-TOPO TA cloning kit according to the manufacturer's protocol and sequenced. The 115-kD STIM1 isoform tagged with YFP and YFP-STIM1L was obtained by cloning the Pml1-Bgl2 fragment from pcDNA-STIM1L into Pml1-BamH1 sites of the SP-YFP-STIM1 plasmid (plasmid 19754; Addgene).

DNA corresponding to exons 11 and 12 from both STIM1S and -L were amplified by PCR (exon 11, Xho1 forward 5'-TTTCTCGAGC-TTCCCTAGCCTGCAGAG-3', and exon 12, BamH1 reverse 5'-GAGA-GGATCCATCCTGCCTACTTCTTAAGAG-3') and inserted into Xho1-BamH1 sites from pEGFP-C1 (BD) to obtain the plasmids GFP-tagged STIM1L or -S C terminus (GFP-STIM1L-C terminal and GFP-STIM1S-C terminal). Exon 11 of STIM1S and -L starts at serine 492. For STIM1S, exon 12 ends at leucine 685 and, for STIM1L, at leucine 791.

### Statistics

A Student's *t* test was used where *p*-values are indicated. Error bars represent SD in Western blot quantification and SEM in Fura-2 experiments. To confirm the results obtained with siSTIM1L1 and siSTIM1S1, each experiment was repeated at least three times with a second siRNA for STIM1S and, for STIM1L, with two additional siRNAs. No significant differences were noted between the effects of the different siRNAs.

### Online supplemental material

Fig. S1 shows STIM1L identification by Western blotting and RACE and the nucleotide sequence of the spliced exon. Fig. S2 shows sequence alignment of the putative alternative splicing domain of STIM1L in several species and confirmation of the presence of two STIM1 mRNAs in myotubes by RT-PCR. Fig. S3 shows Tg-induced SOCE when both STIM1S and Orai1 are silenced in myotubes, Fura-2 fluorescence quench after store depletion when both STIM1S and STIM1L are silenced in myotubes, and STIM1S activation measured by FRET after store depletion. Fig. S4 shows expression of YFP-tagged exons 11 and 12 of STIM1S and -L in myoblasts assessed by Western blotting, Tg-induced SOCE in myoblasts expressing YFP-tagged exons 11 and 12 of STIM1S and -L, and distribution of YFP-STIM1L before and after actin depolymerization with cytochalasin D. Fig. S5 shows the effects of cytochalasin D and latrunculin on STIM1L distribution and the distribution of STIM1S-GFP and Orai1-RFP in store-filled myoblasts. Online supplemental material is available at <http://www.jcb.org/cgi/content/full/jcb.201012157/DC1>.

We thank Drs. S. Treves, N. Demareux, M. Frieden, F. Antigny, and M. Leroy for their comments on the manuscripts. We also thank P. Brawand and C. Pomponio for excellent technical assistance on cell cultures, Drs. A. Kaelin and D. Ceroni for providing muscle biopsies, Dr. Anjana Rao for providing STIM1-YFP plasmids, the Swiss-Prot Group for providing the phylogenetic study, José Maria Rincon Garriz for providing the T cells, Dr. C.J.S. Edgell for providing the EA.hy926 cells, and Drs. D. Al-Ansary and B. Niemeyer for providing the Orai1-RFP construct.

This work was supported by grants from the Fonds National Suisse de la Recherche Scientifique (310030-124910) to L. Bernheim, Fondation Suisse de Recherche sur les Maladies Musculaires, Fondation Hans Wilsdorf, and Fondation Marcel Levaillant.

Submitted: 24 December 2010

Accepted: 23 June 2011

## References

- Arnaudeau, S., N. Holzer, S. König, C.R. Bader, and L. Bernheim. 2006. Calcium sources used by post-natal human myoblasts during initial differentiation. *J. Cell. Physiol.* 208:435–445. doi:10.1002/jcp.20679
- Baba, Y., K. Hayashi, Y. Fujii, A. Mizushima, H. Watarai, M. Wakamori, T. Numaga, Y. Mori, M. Iino, M. Hikida, and T. Kurosaki. 2006. Coupling of STIM1 to store-operated  $\text{Ca}^{2+}$  entry through its constitutive and inducible movement in the endoplasmic reticulum. *Proc. Natl. Acad. Sci. USA.* 103:16704–16709. doi:10.1073/pnas.0608358103
- Baroffio, A., J.P. Aubry, A. Kaelin, R.M. Krause, M. Hamann, and C.R. Bader. 1993. Purification of human muscle satellite cells by flow cytometry. *Muscle Nerve.* 16:498–505. doi:10.1002/mus.880160511
- Berna-Erro, A., A. Braun, R. Kraft, C. Kleinschmitt, M.K. Schuhmann, D. Stegner, T. Wulsch, J. Eilers, S.G. Meuth, G. Stoll, and B. Nieswandt. 2009. STIM2 regulates capacitive  $\text{Ca}^{2+}$  entry in neurons and plays a key role in hypoxic neuronal cell death. *Sci. Signal.* 2:ra67. doi:10.1126/scisignal.2000522
- Berridge, M.J., M.D. Bootman, and H.L. Roderick. 2003. Calcium signalling: dynamics, homeostasis and remodelling. *Nat. Rev. Mol. Cell Biol.* 4:517–529. doi:10.1038/nrml1155
- Brandman, O., J. Liou, W.S. Park, and T. Meyer. 2007. STIM2 is a feedback regulator that stabilizes basal cytosolic and endoplasmic reticulum  $\text{Ca}^{2+}$  levels. *Cell.* 131:1327–1339. doi:10.1016/j.cell.2007.11.039
- Buchthal, F., and H. Schmalbruch. 1980. Motor unit of mammalian muscle. *Physiol. Rev.* 60:90–142.
- Calloway, N., M. Vig, J.P. Kinet, D. Holowka, and B. Baird. 2009. Molecular clustering of STIM1 with Orai1/CRACM1 at the plasma membrane depends dynamically on depletion of  $\text{Ca}^{2+}$  stores and on electrostatic interactions. *Mol. Biol. Cell.* 20:389–399. doi:10.1091/mbc.E07-11-1132
- Caride, A.J., A.G. Filoteo, A.R. Penheiter, K. Pászty, A. Enyedi, and J.T. Penniston. 2001. Delayed activation of the plasma membrane calcium pump by a sudden increase in  $\text{Ca}^{2+}$ : fast pumps reside in fast cells. *Cell Calcium.* 30:49–57. doi:10.1054/ceca.2001.0212
- Cifuentes, F., J. Vergara, and C. Hidalgo. 2000. Sodium/calcium exchange in amphibian skeletal muscle fibers and isolated transverse tubules. *Am. J. Physiol. Cell Physiol.* 279:C89–C97.
- Darbellay, B., S. Arnaudeau, S. König, H. Jousset, C. Bader, N. Demareux, and L. Bernheim. 2009. STIM1- and Orai1-dependent store-operated calcium entry regulates human myoblast differentiation. *J. Biol. Chem.* 284:5370–5380. doi:10.1074/jbc.M806726200
- Darbellay, B., S. Arnaudeau, D. Ceroni, C.R. Bader, S. König, and L. Bernheim. 2010. Human muscle economy myoblast differentiation and excitation-contraction coupling use the same molecular partners, STIM1 and STIM2. *J. Biol. Chem.* 285:22437–22447. doi:10.1074/jbc.M110.118984
- Dirksen, R.T. 2009. Checking your SOCCs and feet: the molecular mechanisms of  $\text{Ca}^{2+}$  entry in skeletal muscle. *J. Physiol.* 587:3139–3147. doi:10.1113/jphysiol.2009.172148
- Ducet, T., C. Vandebrout, M.L. Cao, J. Lebacqz, and P. Gailly. 2006. Functional role of store-operated and stretch-activated channels in murine adult skeletal muscle fibres. *J. Physiol.* 575:913–924. doi:10.1113/jphysiol.2006.115154
- Edwards, J.N., R.M. Murphy, T.R. Cully, F. von Wegner, O. Friedrich, and B.S. Launikonis. 2010. Ultra-rapid activation and deactivation of store-operated  $\text{Ca}^{2+}$  entry in skeletal muscle. *Cell Calcium.* 47:458–467. doi:10.1016/j.ceca.2010.04.001
- Fahrner, M., M. Muik, I. Derler, R. Schindl, R. Fritsch, I. Frischauf, and C. Romanin. 2009. Mechanistic view on domains mediating STIM1-Orai coupling. *Immunol. Rev.* 231:99–112. doi:10.1111/j.1600-065X.2009.00815.x
- Fasolato, C., M. Hoth, and R. Penner. 1993. Multiple mechanisms of manganese-induced quenching of fura-2 fluorescence in rat mast cells. *Pflügers Arch.* 423:225–231. doi:10.1007/BF00374399
- Feske, S. 2009. Orai1 and STIM1 deficiency in human and mice: roles of store-operated  $\text{Ca}^{2+}$  entry in the immune system and beyond. *Immunol. Rev.* 231:189–209. doi:10.1111/j.1600-065X.2009.00818.x
- Feske, S. 2010. CRAC channelopathies. *Pflügers Arch.* 460:417–435. doi:10.1007/s00424-009-0777-5
- Feske, S., C. Picard, and A. Fischer. 2010. Immunodeficiency due to mutations in Orai1 and STIM1. *Clin. Immunol.* 135:169–182. doi:10.1016/j.clim.2010.01.011
- Gorassini, M., T. Eken, D.J. Bennett, O. Kiehn, and H. Hultborn. 2000. Activity of hindlimb motor units during locomotion in the conscious rat. *J. Neurophysiol.* 83:2002–2011.
- Hoth, M., and R. Penner. 1992. Depletion of intracellular calcium stores activates a calcium current in mast cells. *Nature.* 355:353–356. doi:10.1038/355353a0
- Kiehn, O., and T. Eken. 1997. Prolonged firing in motor units: evidence of plateau potentials in human motoneurons? *J. Neurophysiol.* 78:3061–3068.
- Kiehn, O., and T. Eken. 1998. Functional role of plateau potentials in vertebrate motor neurons. *Curr. Opin. Neurobiol.* 8:746–752. doi:10.1016/S0959-4388(98)80117-7
- König, S., V. Hinard, S. Arnaudeau, N. Holzer, G. Potter, C.R. Bader, and L. Bernheim. 2004. Membrane hyperpolarization triggers myogenin and myocyte enhancer factor-2 expression during human myoblast differentiation. *J. Biol. Chem.* 279:28187–28196. doi:10.1074/jbc.M313932200
- Kurebayashi, N., and Y. Ogawa. 2001. Depletion of  $\text{Ca}^{2+}$  in the sarcoplasmic reticulum stimulates  $\text{Ca}^{2+}$  entry into mouse skeletal muscle fibres. *J. Physiol.* 533:185–199. doi:10.1111/j.1469-7793.2001.0185b.x
- Lamb, G.D. 2000. Excitation-contraction coupling in skeletal muscle: comparisons with cardiac muscle. *Clin. Exp. Pharmacol. Physiol.* 27:216–224. doi:10.1046/j.1440-1681.2000.03224.x
- Launikonis, B.S., and E. Ríos. 2007. Store-operated  $\text{Ca}^{2+}$  entry during intracellular  $\text{Ca}^{2+}$  release in mammalian skeletal muscle. *J. Physiol.* 583:81–97. doi:10.1113/jphysiol.2007.135046
- Launikonis, B.S., D.G. Stephenson, and O. Friedrich. 2009. Rapid  $\text{Ca}^{2+}$  flux through the transverse tubular membrane, activated by individual action potentials in mammalian skeletal muscle. *J. Physiol.* 587:2299–2312. doi:10.1113/jphysiol.2009.168682
- Launikonis, B.S., R.M. Murphy, and J.N. Edwards. 2010. Toward the roles of store-operated  $\text{Ca}^{2+}$  entry in skeletal muscle. *Pflügers Arch.* 460:813–823. doi:10.1007/s00424-010-0856-7
- Liou, J., M.L. Kim, W.D. Heo, J.T. Jones, J.W. Myers, J.E. Ferrell Jr., and T. Meyer. 2005. STIM1 is a  $\text{Ca}^{2+}$  sensor essential for  $\text{Ca}^{2+}$ -store-depletion-triggered  $\text{Ca}^{2+}$  influx. *Curr. Biol.* 15:1235–1241. doi:10.1016/j.cub.2005.05.055
- Liou, J., M. Fivaz, T. Inoue, and T. Meyer. 2007. Live-cell imaging reveals sequential oligomerization and local plasma membrane targeting of stromal interaction molecule 1 after  $\text{Ca}^{2+}$  store depletion. *Proc. Natl. Acad. Sci. USA.* 104:9301–9306. doi:10.1073/pnas.0702866104
- Luik, R.M., M.M. Wu, J. Buchanan, and R.S. Lewis. 2006. The elementary unit of store-operated  $\text{Ca}^{2+}$  entry: local activation of CRAC channels by STIM1 at ER-plasma membrane junctions. *J. Cell Biol.* 174:815–825. doi:10.1083/jcb.200604015
- Lyfenko, A.D., and R.T. Dirksen. 2008. Differential dependence of store-operated and excitation-coupled  $\text{Ca}^{2+}$  entry in skeletal muscle on STIM1 and Orai1. *J. Physiol.* 586:4815–4824. doi:10.1113/jphysiol.2008.160481
- McCarl, C.A., C. Picard, S. Khalil, T. Kawasaki, J. Röther, A. Papalos, J. Kutok, C. Hivroz, F. Ledeist, K. Plogmann, et al. 2009. Orai1 deficiency and lack of store-operated  $\text{Ca}^{2+}$  entry cause immunodeficiency, myopathy, and ectodermal dysplasia. *J. Allergy Clin. Immunol.* 124:1311–1318.e7. doi:10.1016/j.jaci.2009.10.007
- Mercer, J.C., W.I. Dehaven, J.T. Smyth, B. Wedel, R.R. Boyles, G.S. Bird, and J.W. Putney Jr. 2006. Large store-operated calcium selective currents due to co-expression of Orai1 or Orai2 with the intracellular calcium sensor, Stim1. *J. Biol. Chem.* 281:24979–24990. doi:10.1074/jbc.M604589200
- Miledi, R., I. Parker, and G. Schalow. 1977. Calcium transients in frog slow muscle fibres. *Nature.* 268:750–752. doi:10.1038/268750a0
- Miledi, R., I. Parker, and P.H. Zhu. 1982. Calcium transients evoked by action potentials in frog twitch muscle fibres. *J. Physiol.* 333:655–679.
- Muik, M., M. Fahrner, I. Derler, R. Schindl, J. Bergsmann, I. Frischauf, K. Groschner, and C. Romanin. 2009. A cytosolic homomerization and a modulatory domain within STIM1 C terminus determine coupling to Orai1 channels. *J. Biol. Chem.* 284:8421–8426. doi:10.1074/jbc.C800229200
- Navarro-Borelly, L., A. Somasundaram, M. Yamashita, D. Ren, R.J. Miller, and M. Prakriya. 2008. STIM1-Orai1 interactions and Orai1 conformational changes revealed by live-cell FRET microscopy. *J. Physiol.* 586:5383–5401. doi:10.1113/jphysiol.2008.162503
- Parekh, A.B., and J.W. Putney Jr. 2005. Store-operated calcium channels. *Physiol. Rev.* 85:757–810. doi:10.1152/physrev.00057.2003
- Park, C.Y., P.J. Hoover, F.M. Mullins, P. Bachhawat, E.D. Covington, S. Raunser, T. Walz, K.C. Garcia, R.E. Dolmetsch, and R.S. Lewis. 2009. STIM1 clusters and activates CRAC channels via direct binding of a cytosolic domain to Orai1. *Cell.* 136:876–890. doi:10.1016/j.cell.2009.02.014



- Picard, C., C.A. McCarl, A. Papolos, S. Khalil, K. Lüthy, C. Hivroz, F. LeDeist, F. Rieux-Laucat, G. Rechavi, A. Rao, et al. 2009. STIM1 mutation associated with a syndrome of immunodeficiency and autoimmunity. *N. Engl. J. Med.* 360:1971–1980. doi:10.1056/NEJMoa0900082
- Prakriya, M., S. Feske, Y. Gwack, S. Srikanth, A. Rao, and P.G. Hogan. 2006. Orai1 is an essential pore subunit of the CRAC channel. *Nature*. 443:230–233. doi:10.1038/nature05122
- Rekling, J.C., G.D. Funk, D.A. Bayliss, X.W. Dong, and J.L. Feldman. 2000. Synaptic control of motoneuronal excitability. *Physiol. Rev.* 80:767–852.
- Roos, J., P.J. DiGregorio, A.V. Yeromin, K. Ohlsen, M. Lioudyno, S. Zhang, O. Safrina, J.A. Kozak, S.L. Wagner, M.D. Cahalan, et al. 2005. STIM1, an essential and conserved component of store-operated  $\text{Ca}^{2+}$  channel function. *J. Cell Biol.* 169:435–445. doi:10.1083/jcb.200502019
- Stein, R.B., J. Bobet, M.N. Ögüztörel, and M. Fryer. 1988. The kinetics relating calcium and force in skeletal muscle. *Biophys. J.* 54:705–717. doi:10.1016/S0006-3495(88)83006-6
- Stiber, J., A. Hawkins, Z.S. Zhang, S. Wang, J. Burch, V. Graham, C.C. Ward, M. Seth, E. Finch, N. Malouf, et al. 2008. STIM1 signalling controls store-operated calcium entry required for development and contractile function in skeletal muscle. *Nat. Cell Biol.* 10:688–697. doi:10.1038/ncb1731
- Treves, S., M. Vukcevic, J. Griesser, C.F. Armstrong, M.X. Zhu, and F. Zorzato. 2010. Agonist-activated  $\text{Ca}^{2+}$  influx occurs at stable plasma membrane and endoplasmic reticulum junctions. *J. Cell Sci.* 123:4170–4181. doi:10.1242/jcs.068387
- Wang, Y.J., X.X. Deng, Y.D. Zhou, E. Hendron, S. Mancarella, M.F. Ritchie, X.D. Tang, Y. Baba, T. Kurosaki, Y. Mori, et al. 2009. STIM protein coupling in the activation of Orai channels. *Proc. Natl. Acad. Sci. USA*. 106:7391–7396. doi:10.1073/pnas.0900293106
- Wu, M.M., J. Buchanan, R.M. Luik, and R.S. Lewis. 2006.  $\text{Ca}^{2+}$  store depletion causes STIM1 to accumulate in ER regions closely associated with the plasma membrane. *J. Cell Biol.* 174:803–813. doi:10.1083/jcb.200604014
- Yuan, J.P., W. Zeng, M.R. Dorwart, Y.J. Choi, P.F. Worley, and S. Muallem. 2009. SOAR and the polybasic STIM1 domains gate and regulate Orai channels. *Nat. Cell Biol.* 11:337–343. doi:10.1038/ncb1842
- Zeng, W., J.P. Yuan, M.S. Kim, Y.J. Choi, G.N. Huang, P.F. Worley, and S. Muallem. 2008. STIM1 gates TRPC channels, but not Orai1, by electrostatic interaction. *Mol. Cell*. 32:439–448. doi:10.1016/j.molcel.2008.09.020
- Zhao, X., M. Yoshida, L. Brotto, H. Takeshima, N. Weisleder, Y. Hirata, T.M. Nosek, J. Ma, and M. Brotto. 2005. Enhanced resistance to fatigue and altered calcium handling properties of sarcalumenin knockout mice. *Physiol. Genomics*. 23:72–78. doi:10.1152/physiolgenomics.00020.2005
- Zhou, Y.D., S. Mancarella, Y.Y. Wang, C.Y. Yue, M. Ritchie, D.L. Gill, and J. Soboloff. 2009. The short N-terminal domains of STIM1 and STIM2 control the activation kinetics of Orai1 channels. *J. Biol. Chem.* 284:19164–19168. (published erratum appears in *J. Biol. Chem.* 2009. 284:25459) doi:10.1074/jbc.C109.010900